Evaluation of Hydrodynamic Force Coefficients in Presence of Biofouling on Marine/Offshore Structures, a Review and New Approach

Franck Schoefs, Arash Bakhtiari, Hamed Ameryoun

Journal of
Marine Science and Engineering

MDPI

Review

Evaluation of Hydrodynamic Force Coefficients in Presence of Biofouling on Marine/Offshore Structures, a Review and New Approach

Franck Schoefs [1,*], Arash Bakhtiari [1] and Hamed Ameryoun [2]

[1] Institut de Recherche en Génie Civil et Mécanique (GeM)-UMR CNRS 6183, Institut Universitaire Mer et Litto-ral (IUML)-FR CNRS 3473, Nantes Université, 44035 Nantes, France; arash.bakhtiari@univ-nantes.fr
[2] CAPACITES SAS Nantes, 2 rue de la Houssinière, 44200 Nantes, France; hamed.ameryoun@capacites.fr
* Correspondence: franck.schoefs@univ-nantes.fr

Abstract: Novel attempts to optimize the design and requalification of offshore structures draws attention to the importance of updating information about the environmental forces. One of the important steps to design or re-assess offshore structures is the re-evaluation/evaluation of bio-colonization's effects. This paper presents a review of studies that considered biofouling in marine/offshore structures. Most of the previous researchers conducted the effects of biofouling as a surface roughness; however, some others proved that despite the surface roughness, other marine fouling components such as surface coverage ratio, biofouling species, and aggregation, may significantly influence hydrodynamic force coefficients, particularly at higher Reynolds numbers (Re). In addition, a new approach is proposed in this paper to estimate the drag coefficient of circular members covered by biofouling. The new approach relies on a multiple parameter equation and builds on the existing measurement of the drag force coefficient. Two relationships between biofouling parameters and drag coefficient are given for hard biofouling at the post-critical Re regime.

Keywords: biofouling; relative surface roughness; drag coefficient; multiple parameter analysis

Citation: Schoefs, F.; Bakhtiari, A.; Ameryoun, H. Evaluation of Hydrodynamic Force Coefficients in Presence of Biofouling on Marine/Offshore Structures, a Review and New Approach. *J. Mar. Sci. Eng.* **2022**, *10*, 558. https://doi.org/10.3390/jmse10050558

Academic Editors: Yuriy Semenov, Alexander Korobkin and Baoyu Ni

Received: 26 February 2022
Accepted: 12 April 2022
Published: 20 April 2022

1. Introduction

Offshore structures in the marine environment suffer from the corrosion and bio-colonization effects (biofouling). Generally, biofouling can be divided into hard, soft and long flapping (Figure 1). The roughness turbulence generated by all the fouling's types is dissimilar [1]. Biofouling can reach a considerable extent depending on the site location and water depth [2–5]. They grow rapidly in the beginning, but growth tapers off after a few years [6]. In the majority of cases, several types of biofouling communities are colonized on the surface of the structure, however, normally there are dominant species and types. Dominant communities and similar species are likely to have similar characteristics (e.g., roughness, weight). Figure 2 depicts two examples of zonal and vertical distribution likely growth on offshore structures for the southern North Sea. Generally, biofouling found in locations could be characterized by different environmental conditions such as light availability, flow speed, and water depth. For example, kelps are limited to the near-surface area since light for photosynthesis is a key factor [7].

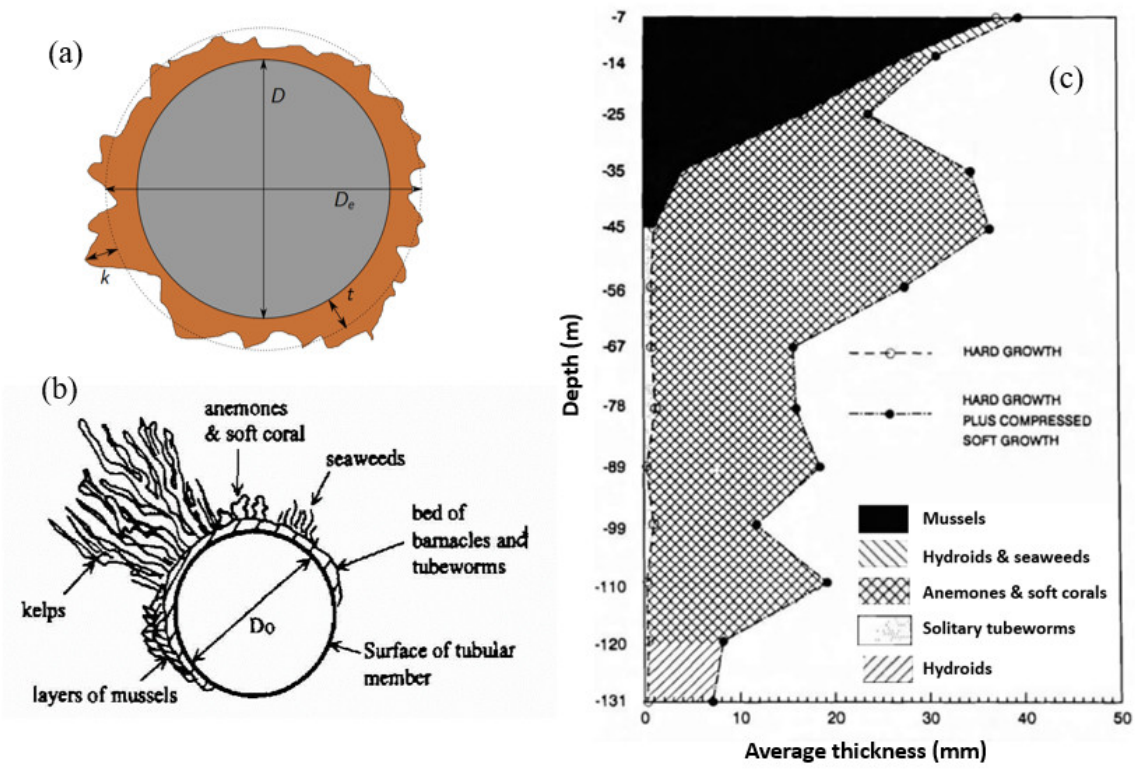

Figure 1. Modification of the external surface of a circular cylinder by biofouling, (**a**) definition of relative surface roughness by *k*: height and *t*: thickness, (**b**) schematic view of soft and hard biofouling (adapted from [8]), and (**c**) thickness variation pattern with the indication of the vertical distribution for North Sea (adapted from [5]).

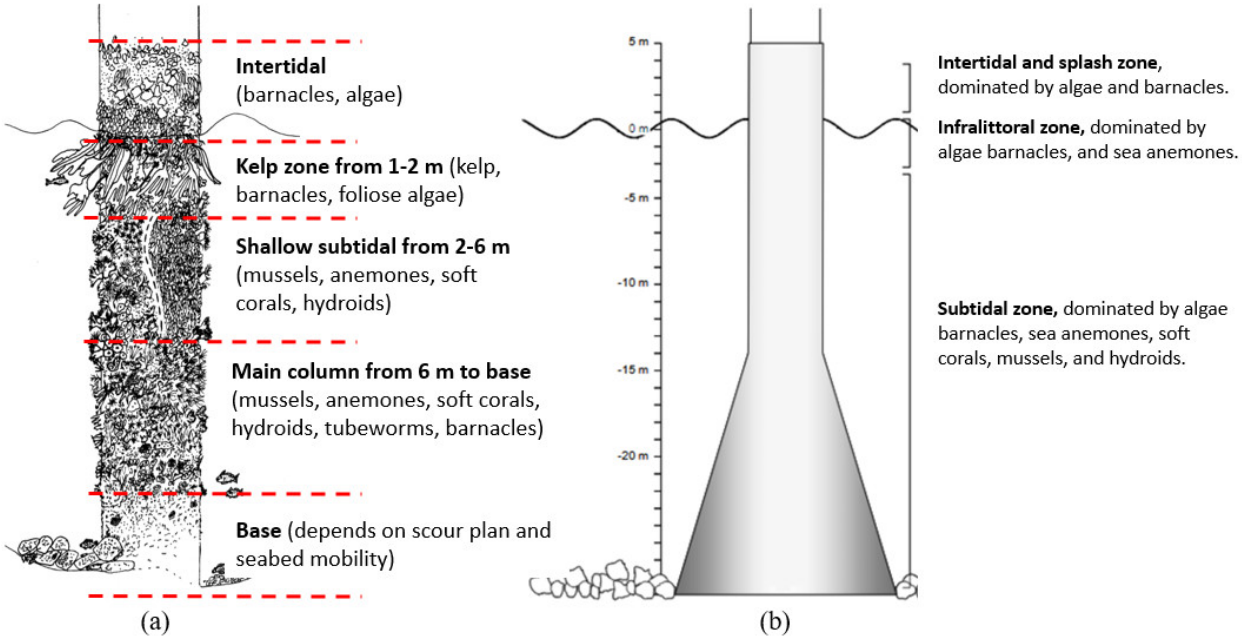

Figure 2. Schematic view of zonal communities and vertical distribution likely on offshore structures in the southern North Sea adopted from (**a**) [7]; (**b**) [9,10].

The inherent randomness of biofouling and its uncertainties make modelling of this environmental loading much more complicated. The most challenging issue is to efficiently predict the structural effects and the value of fluid force coefficients. The most common

approach was considering the influence of biofouling as a surface roughness [11–17]. Authors have focused on this roughness by considering several species and carrying out new tests [18,19]. Others have modelled this roughness and provided frameworks where it can be introduced in a loading computation [20–22].

The pioneering works of Sarpkaya [14,15] concern fixed cylinders with a uniformly distributed surface roughness and placed in a sinusoidal oscillating flow. Different relative roughness values without considering the roughness density have been tested in a range of 1/240 to 1/50. Rodenbusch and Källström [13] consider fully roughened cylinders subjected to sinusoidal oscillation in a large basin propagating two-dimensional flow. Another method of experimentation concerns the technique of forced sinusoidal oscillations for cylinders in a basin [11,12,18,19]. A number of studies also tried to explore the marine fouling effects on the cylinders oscillation [23–26]. Gaurier et al. [27] showed an increase of 10% for drag forces in presence of meso roughness over macro-roughness. In a novel study, Zeinoddini et al. [28] conducted a comprehensive review on vortex shedding behind stationary and non-stationary cylinders with surface roughness. In addition, they conducted some new experiments on fully covered circular cylinders with regular single-size pyramidal protrusions to model the biofouling effects. They proved that the cylinder dynamical behaviour and fluid forces are significantly affected in the vicinity of the surface protrusions.

Most of the aforementioned studies assumed that the roughness density is uniform/semi-uniform and the cylinder is fully covered. Even in these "controlled laboratory conditions", significant differences in drag, inertia and lift coefficients data has been found (especially for Keulegan-Carpenter higher than 8) with no predominant reason [17]; however it may be due to the 3D vortex instability affecting these coefficients. Moreover, API-RP-2A [6] noted that the relative roughness ratio e ($e = k/D$, where k is the average peak-to-valley and D is the structure dimension) from biofouling on offshore tubular structures is generally greater than 10^{-3} and in some cases may exceed 10^{-2}. These are significantly higher than that for normal cylinders, which led to a change in the Strouhal number (St) [16,29]. On the other hand, a specific work carried out by Theophanatos [30] pointed out that the one-parameter characterization of roughness, i.e., k/D may not be suitable for embracing all the complexity of fluid-structure interactions nor for quantifying hydrodynamic loadings precisely. In fact, parameters such as roughness shape (geometry), effects of soft seaweeds, limitation of experimental scales and percentage of coverage have been shown to have a great influence on results and should be taken into account. More recently, Zeinoddini et al. [28,31] conducted some experiments on cylinders covered by regular single-size hemispherical protrusions with three different coverage ratios. Based on their results, for an oscillating cylinder under the VIV effect (Vortex Induced Vibration), the coverage ratio had small effects on the drag coefficient; however, lift coefficient and cylinders with lower coverage ratios had lower peak amplitudes and had narrower lock-in ranges. The shape of the protrusions (pyramidal or hemispherical) was reported to have also small impacts on the peak oscillation amplitude and on the maximum lift and drag coefficients [28].

As noted above, previous studies proved that despite the relative surface roughness, other marine fouling parameters such as fouling geometry, density, hard/soft species, colonization pattern, and surface coverage ratio, may significantly influence the hydrodynamic coefficients of a cylindrical member, particularly at higher Reynolds numbers (Re). These parameters are prerequisite parameters for defining marine fouling effects on hydrodynamic force coefficients. However, there are still gaps in design criteria knowledge for influential parameters of hard biofouling and of other biofouling species; therefore, potential impacts are not fully understood. This paper reviews these areas in the light of available data published in the literature and an understanding of the problems.

In general, the main aim of the present work is to enhance the knowledge of hydrodynamic forces in a circular member under a steady/oscillating current by considering all the influential biofouling factors. Particular attention was paid to the influence of the

roughness ratio, surface coverage ratio, colonization pattern (aggregation), and biofouling species. Moreover, gathered data from a number of experiments concerned with the effects of biofouling and surface roughness on the drag coefficient were reviewed and analyzed.

2. Biofouling Modelling

2.1. Surface Roughness Parameter

Biofouling is a major (both economic and technical) issue for nearly all marine industries such as oil and gas, marine renewable energy, pipelines and cables, ships, aquaculture and wave power facilities [32]. Therefore, several research programs have been carried out for including biofouling effects in the designs and the operation stages. As stated before, most researchers treated fouling as a kind of surface roughness [5,8,24,25,33–36]. These studies constitute parts of a wider topic of the effects of surface roughness on the flow around cylinders. In general, surface irregularities significantly change the flow regime around a cylindrical body [37–41].

With a smooth circular cylinder, the drag coefficient C_D is dependent on the Reynolds number. As the flow enters the critical regime, an abrupt drop in C_D is experienced [42]. This phenomenon is called the drag crisis and occurs because the boundary layer turns turbulent in this flow regime and the separation points move downstream. The wake, therefore, narrows down and the drag and lift coefficients are reduced (Figure 3). Bearman and Harvey [38] reported that surface dimples reduce the drag force by lowering the critical Reynolds number Re at which flow becomes turbulent. This type of finding was applied for instance in the design and production of sports balls [43]. As illustrated in Figure 3, the drag coefficient for rough cylinders in Sarpkaya experiments in harmonic flow [16], however, was twice as great in comparison to smooth cylinders. It also grew with the relative roughness $e = k/D$. We notice also the role of the Keulegan–Carpenter number KC, defined in presence of marine growth by Boukinda [2], which is discussed further in the paper. However, there are some contradictory findings, for example, drag coefficients in wind tunnel experiments on steel tubes covered with artificial and real marine roughness showed almost no variation with Re [44].

Buresti [29] found that with a high level of surface roughness the vortex shedding mechanism is not disturbed, but it is stabilized and grows stronger. The critical regime can be impressively reduced by the roughness, and it may even disappear in the case of cylinders with high roughness. It was demonstrated that strong supercritical and post-critical vortex shedding can take place from highly, but uniformly, roughened circular cylinders. Experiments on artificially roughened cylinders showed that the surface roughness resulted in the significant span-wise coherence of vortex shedding and large drag and lift forces [33].

Ribeiro [45] found that smooth flow around rough circular cylinders (at relatively low Re values) had larger root-mean-square (RMS) and peak fluctuating values of the lift coefficient and of pressure coefficients than those compared to smooth circular cylinders at high Re values. Span-wise cross-correlation measurements of the pressures revealed a correlation length, depending on the roughness type, of around 3D or 4D in the smooth flow tests.

Basu [46] presented the C_D in the subcritical, critical, and post-critical Re regimes together as a function of surface roughness (Figure 4). He showed that there are different patterns of drag fore variation versus surface roughness ratio in the subcritical, critical, and post-critical Re regimes.

It is worth mentioning for most offshore structures in extreme conditions, Re is well integrated into the post-critical flow regime, where the steady flow drag coefficient (C_{Ds}) for circular cylinders is independent of Reynolds numbers (API-RP-2A, 2010). The dependency of C_{Ds} at post-critical Re and on relative surface roughness from several studies is shown in Figure 5 for roughness surface induced by "hard" marine growth and data presented in Table 1.

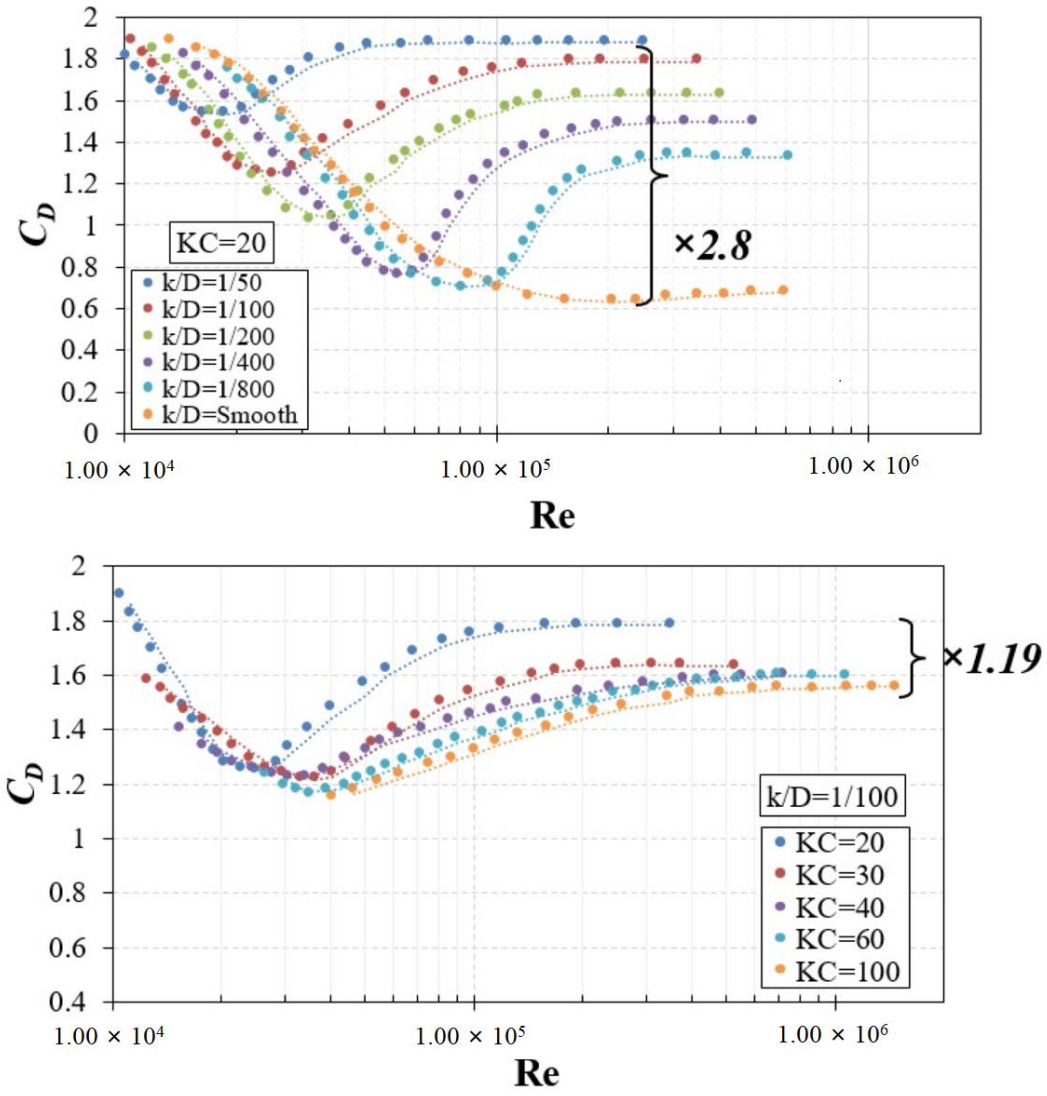

Figure 3. Drag coefficient for a fixed circular cylinder for steady flow in critical flow regime, for various roughness ratios (rebuilt with data from [16]).

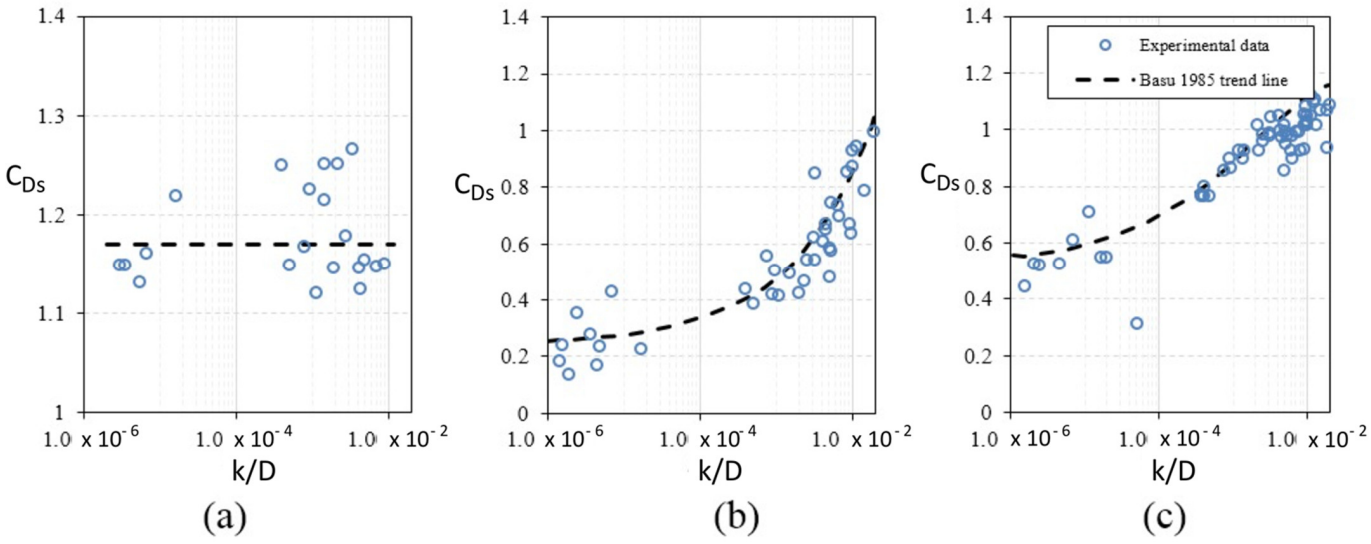

Figure 4. Variation of the mean drag coefficient with surface roughness ratio for (**a**) subcritical, (**b**) critical, and (**c**) post-critical ranges of Reynolds number (rebuilt with data from [46]).

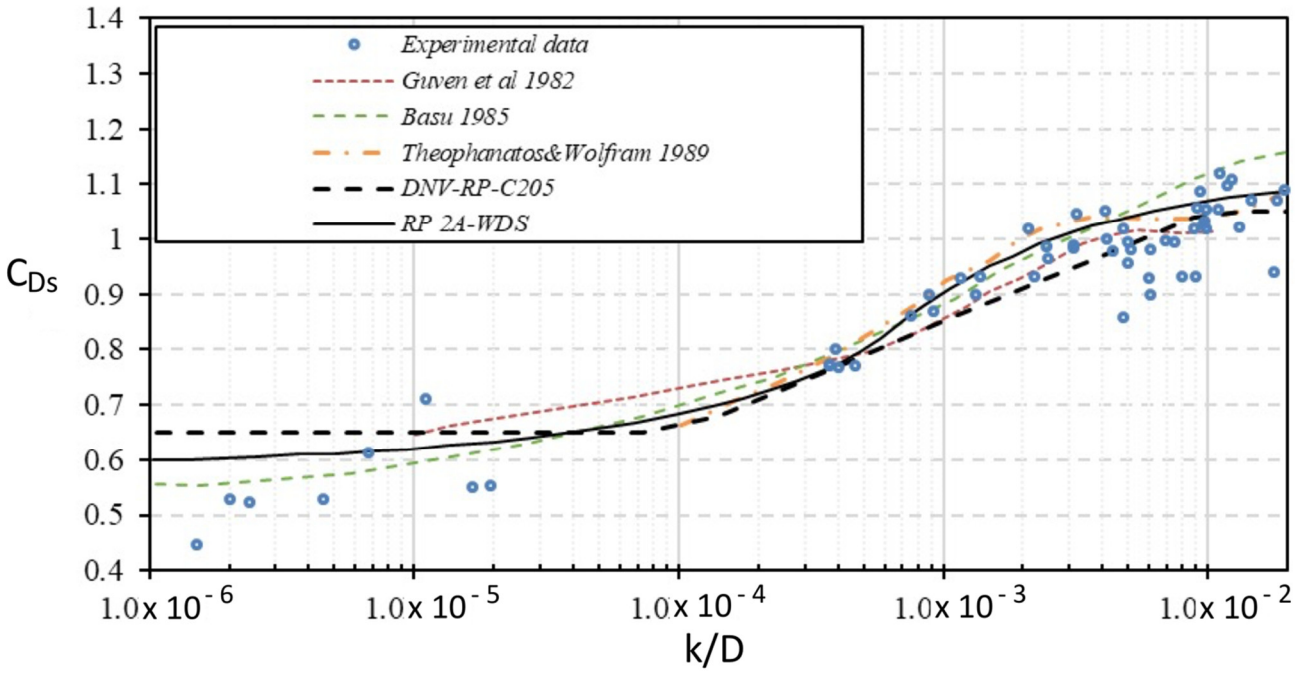

Figure 5. Variation of the mean drag coefficient with relative roughness from some researchers.

Table 1. Details of some laboratory experiments on flow over a circular cylinder.

Author and Dates	Re ($\times 10^4$)	K/D ($\times 10^{-3}$)	Coverage Ratio	Reference
Achenbach (1971, 1977)	2.2 to 400	0 to 9	100%	[47,48]
Guven et al. (1980)	7 to 55	2.5 to6.2	100%	[49]
Buresti (1981)	2.6 to 28.8	1 to 12	100%	[29]
Nakamura and Tomonari (1982)	4 to 170	0.065 to 10	100% and partially	[50]
Rooney and Peltzer (1982)	15 to 40	1 to 2.2	100%	[51]
Nath (1982)	3 to 50	20	100%	[44]
Wolfram and Theophanatos (1985)	10 to 100	5 to 98	25%, to 100%	[33]
Theophanatos and Wolfram (1989)	12 to 100	5 to 98	5% to 100%	[18]
Jubran et al. (1990)	0.6 to 4.6	5.75 to 21.5	100%	[52]
Ribeiro (1991a, 1991b)	5 to 40	1.8 to 12.3	100%	[45,53]
Bearman and Harvey (1993)	2 to 30	4.5 and 9	100%	[38]
Cheung and Melbourne (1995)	6 to 100	0.021 to 2.3	100	[54]
Uematsu and Yamada (1995)	0.25 to 8.76	0.19 to 3	100%	[55]
Wolfram and Naghipour (1999)	up to $\times 100$	38	100%	[56]
Nedrebø (2014)	0.216 to 1.94	10 to 70	100%	[25]

Table 1. *Cont.*

Author and Dates	Re ($\times 10^4$)	K/D ($\times 10^{-3}$)	Coverage Ratio	Reference
Butt and Egberds (2013)	3.14 to 27.7	19.8	100%	[41]
Gao et al. (2015)	2.5 to 18	0.11 and 12	100%	[57]
Zhou et al. (2015)	0.74 to 1.8	50	100%	[58]

The experimental data plotted in Figure 6 were obtained from the studies with 100% coverage, which are mentioned in Table 1. As it can be seen from Figure 6, the roughness ratio varies from 1×10^{-6} (smooth cylinder) to 2×10^{-2} while the drag coefficient approximately changes from 0.5 to 1.1. All these data were presented for members with a fully covered surface and semi-uniform/uniform distribution of surface roughness. However, they do not include the areal density of roughness and well documented (size) shape of the roughness. Both factors play a key role [59–61].

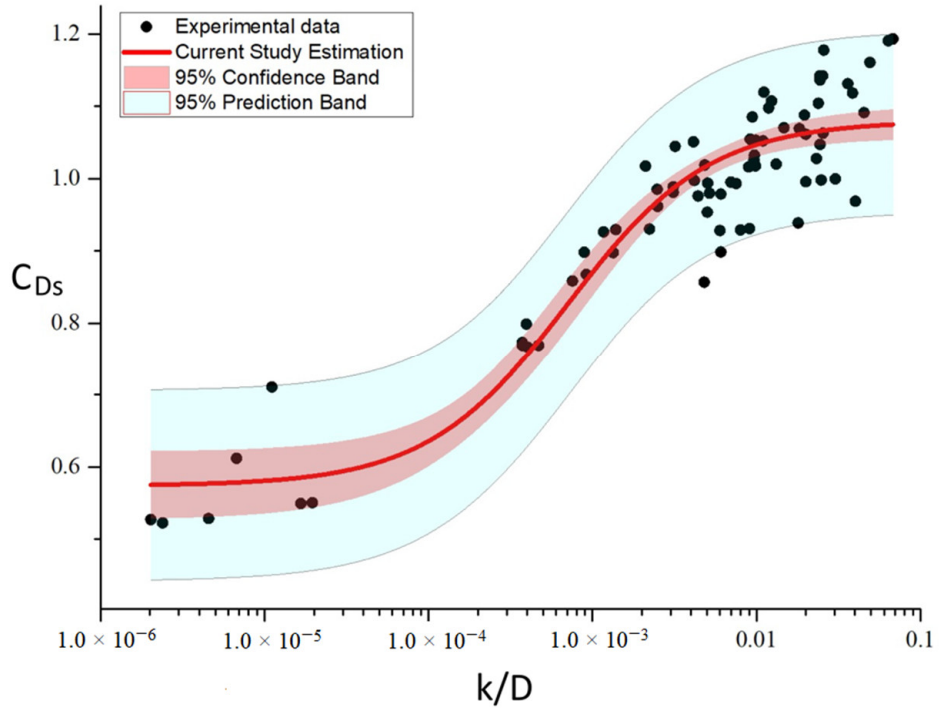

Figure 6. Variation of the C_{Ds} with surface roughness ratio and the 95% confidence intervals (red region) around the fit.

Reviewed studies proved that both C_{Ds} and C_D are reasonably dependent on (k/D) in the post-critical regime [46]. For fitting the data, we have selected a structure of a function that respects the physical meaning of the trends and the asymptotic behaviours. First, the exponential function is known to fit very well data with asymptotic behaviour: that is the main mathematical structure of the model. Second for $k/D = 0$, C_{Ds} reach 0.6 for a smooth cylinder. Third, a classical ratio function is used for fitting the S shape structure (moderate-high-moderate slopes of the curve). Then 2 remaining parameters were fitted by using a minimizing the mean square error; the optimization problem was solved by using a simplex method with 2 parameters to be identified.

In this paper, in order to find the dependence of the C_{Ds} on surface roughness, the exponential function of a ratio was selected for giving the best match with the measured data which is presented in Equation (1).

$$C_{Ds} = e^{-(0.071+\frac{2.9\times10^{-4}}{(\frac{k}{D})-4.12\times10^{-4}})} \quad (1)$$

where k/D is the surface roughness ratio.

Figure 6 shows a curve-fit to the experimental data. It should be noted that the fitted curves are only valid for the data range. In Figure 6, the values of C_{Ds} in lower surface roughness ratios (considered as a smooth cylinder) are around 0.6. The maximum C_{Ds} value is represented by the curve shown in this figure, i.e., the value of C_{Ds} is about 1.05. In comparison with Figure 5, the trend of the fitted curve by the current study is fairly well in compliance with the findings of other researchers. With lower surface roughness ratios, the fitted curve seems to be somehow underpredicted (approximately 5% lower rather than the standard values). It is reasonable to expect the C_D to be asymptotic to some value for cylinders with a smooth surface ($k/D < 4 \times 10^{-4}$).

Based on Figures 5 and 6, one may conclude that in higher relative roughness, experimental data are scattered in a wider band and even went beyond the confidence intervals and prediction bands (Figure 5). Figure 6 shows that the variation of C_{Ds} around the maximum surface roughness ($0.01 < k/D < 0.1$) is about $\pm$10% of the curve value which leads to ranges of maximum values of about 0.95 to 1.2.

The presented regression model was evaluated by visualizing residual plots according to Figure 7. Figure 7a depicts a histogram of raw residuals that is plotted to examine whether the observations are randomly sampled from a normal distribution. However, for small datasets detecting normality from a histogram could be difficult. Therefore, the residual values of the fitted curve are plotted in Figure 7b to identify substantive departures from normality.

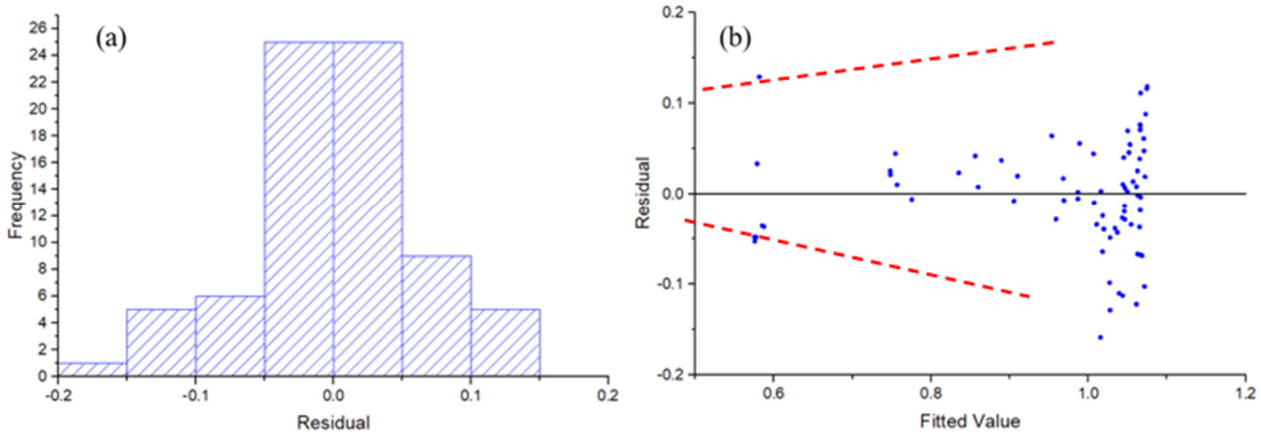

Figure 7. Residual plots of the single parameter model (**a**) residual histogram plot, (**b**) normal residual of the fitted curve (calculated value subtracted by measured value).

Based on Figure 7a, the histogram of the residuals is distributed with a symmetric bell-shaped histogram, which is distributed around zero; the standard deviation is about 0.06. However, the residuals of fitted values (see the red dashed line in Figure 7b) have an increasing trend which suggests that the error variance increases with increasing the drag coefficient (i.e., with increasing the k/D). This indicates that the assumption of dependency of C_{Ds} only on relative surface roughness might not likely be reliable and the one-parameter regression is not an appropriate approach in this case. It should be noticed that in this set of data (Figure 7) the number of measured values for $C_{Ds} < 0.8$ is not equal to the higher C_{Ds}.

It can be considered as an error of modelling and several explanations can rise up for this scattered data; however, the main conclusion is that there are some other parameters

that should be taken into account such as experimental setup, roughness geometry, and its distribution. For example, Achenbach [48] and Buresti [30] simulated the roughness by glueing emery papers to the cylinder surface while Batham [62] utilized solid particles such as glass beads or sandpapers and Sarpkaya [16] considered sand-roughened cylinders with a semi-uniform distribution. Finally, this error of modelling is shown to vary with C_{Ds}. The residuals vary from ± 0.07 to ± 0.15 for the drag coefficients in steady flow varying, respectively, from 0.6 to 1.05 in this paper leading to a relative uncertainty is between 12 and 14%. This result is fundamental when propagating uncertainties in structural reliability assessment [22]. However, for providing a more accurate model of error, more tests for $k/D < 2.10^{-3}$ are needed.

2.2. Complementary Influential Parameters

Most of the previous studies have related to the effect of surface roughness on the hydrodynamic coefficients, with the assumption of the existence of hard biofouling. Only a few numbers of researchers have studied the effects of soft and long flapping biofouling. Theophanatos [31] examined the effects of the kelp and soft biofouling on the drag coefficient. He provided a new roughness definition based on the length of the kelp same as that calculated with hard biofouling $e = l/D$, where l is the average length of the kelp and D is the component dimension. The drag coefficient with the fully kelp covered cylinders grew up to 40% greater than the fully mussel covered cylinders [31]. Moreover, as illustrated in Table 2, the effect of a mixture of biofouling was also tested and show a large scatter depending on the angle of current attack.

Table 2. Summary of soft and mixed fouling test results [31].

Biofouling Type and Relative Angle of Particle Velocity	D (mm)	Surface Cover	k_{min}	C_D
Bare cylinder	400	0	0	0.49
Sea Anemones				
Non-uniform	400	40	60	1.19
Uniform	400	25	60	1.15
Sea anemones and tunicates				
$\theta^* = 0$	315	70	20–80	1.35
$\theta = 90$	315	70	20–80	1.09
Barnacles, mussels, and seaweed				
$\theta = 0$	315	35	24	1.11
$\theta = 180$	315	35	24	1.03
$\theta = 0$	400	45	24	0.92
$\theta = 0$	400	45	24	1.1

Table 2 depicts that with the mixture of soft and hard biofouling the drag coefficient varies significantly from those from the pure soft fouling. Nedrebø [25], in a separate study, investigated the variation in the drag coefficient for the soft type of surface roughness. The results of these researches proved that the drag coefficient has been significantly different from those obtained for an equivalent hard roughness. Theophanatos [31] results revealed that the drag coefficient increased for various species; it was about 1.4 times greater for fully kelp covered cylinders compared to cylinders fully covered with single layer mussels. Nedrebø [25] did the same conclusion for the soft surface roughness such as carpet. Theophanatos and Wolfram [18] also demonstrated through experimental trials that the biofouling species (hard, soft, and long flapping) alter the trends of drag coefficient as a function of surface roughness ratio (l/D) and surface coverage ratio.

Despite the biofouling species, there is another important factor regarding the biofouling effect on the loading of the offshore structure; the percentage of the member's surface, which is covered by biofouling. This parameter is termed "coverage percentage". After submergence in seawater, a circular cylinder may experience biofouling coverage ratios of zero up to 100%. The coverage percentage depends on several parameters such as the geographical location, temperature, water depth, currents, waves, temperature, nutrients, light, submergence duration, whether anti-fouling agents are used or not, etc. [63]. In addition, Achenbach and Heinecke [38] and Ribeiro [46,54] found that roughness density plays a critical role in the mean forces and pressures. Fuss [40] showed that in addition to the maximal and mean surface roughness, the surface skewness is a further roughness parameter, which affects the critical Reynolds number and the lift/drag coefficients. As an example, Table 3 summarizes the coverage ratios reported by Vedaprakash et al. [64]. Figure 8 shows another illustration of a colony of barnacles, which is partially covering a submerged surface.

Table 3. Biofouling observations on metals sheets immersed in 3 m of seawater for 185 and 390 days, Ennore Port [64].

	Titanium	Stainless Steel	Galvanised Steel	Copper Nickel
Coverage after 185 Days (%)	90.8	73.8	19.4	0.3
Coverage after 390 Days (%)	87.2	93.2	88.4	25.1

Figure 8. A photo on partial coverage by a colony of barnacles on a biofouled surface (https://www.marineinsight.com accessed on 25 February 2022).

Theophantatos and Wolfram [18] proved that surface cover increases in hydrodynamic drag in a nonlinear relation. They showed that with the lower coverage percentage the member acts as some segmental members. In a case where larger portions of the member are free of biofouling, the member is treated as a series of the cylindrical segment by applying a local drag coefficient. Zeinoddini et al. [32] also confirmed this short conclusion. Moreover, based on Theophanatos [31] investigations, a different type of biofouling (hard, soft and long flapping) resulted in different curves of drag coefficient as a function of coverage ratio (Figure 9).

Some researchers have investigated the drag coefficient as a linear regression function of the thickness and roughness [65]. Güven et al. [50] reported that when the roughness grew larger than the thickness of the boundary layer a thicker and more retarded boundary layer was formed. The roughness effect on the flow depends on the relative size of the roughness to the boundary layer thickness, which is different from the effect of the relative

size of the roughness to the cylinder diameter [66]. According to API [6], an additional parameter that affects the drag coefficient of elements with circular cross-sections is the effective diameter (Figure 1a).

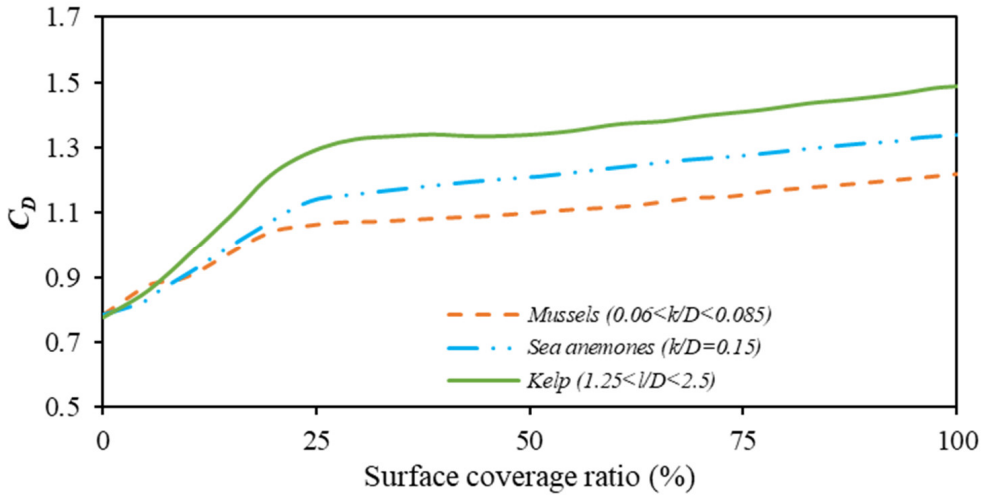

Figure 9. Evolution of drag coefficient (C_D) as a function of biofouling coverage ratio for different surface roughness values (k) and biofouling type (adapted from [31]).

By growing the thickness of biofouling, the effective diameter of the cylinder changes with time [67,68]. To calculate the effective diameter values, it should be assumed that cylinders surfaces or at least a substantial part of them are completely covered with biofouling. In cases where the surface coverage ratio experiences a lower percentage of biofouling, especially if the coverage percentage is less than 50%, this definition should be considered with more scepticism. Figure 10 depicts the Theophanatos data on multiple layers of hard biofouling in comparison with a single layer case for the same k/D = 0.06 and for different surface coverage percentages [31]. As this figure shows, the C_D value increases up to about 1.5 times greater than the single-layer colonized biofouling.

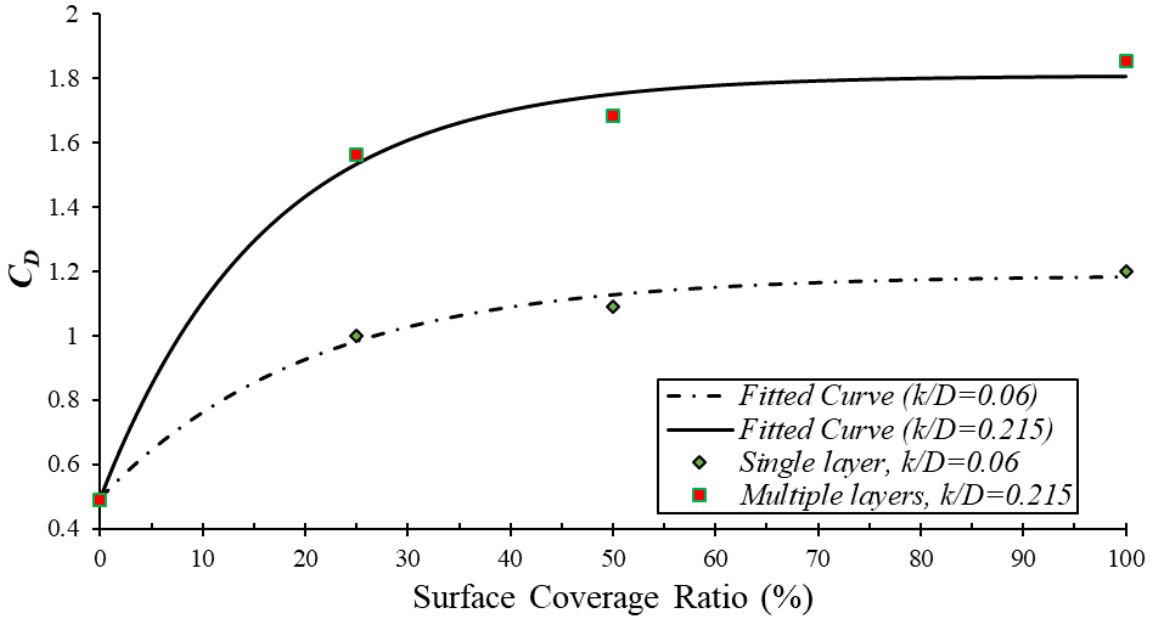

Figure 10. Evolution of drag coefficient (C_{Ds}) as a function of surface coverage ratio for different aggregation patterns (rebuilt from data of [31]).

3. Evaluation of Existing Data Using Multiple Parameter Approach

Section 2 focused on the evaluation of the drag coefficient versus the influential parameters as individual components. However, none of those functions provided a general estimation of the C_D or C_{Ds}. On the other hand, when the drag coefficient is being estimated using the methods of combined biofouling parameters, it might influence the magnitude of the C_{Ds}. For example, surface roughness increases the drag coefficient and consequently the net force. However, the effects of the surface coverage ratio on the C_{Ds} might be different, when the surface roughness is changing. On the other hand, there is some lake of data in the present database, for instance, the only available data published on multi-layer biofouling cases were presented only in one relative surface roughness.

Therefore, the interaction of the mentioned parameters makes the estimation of the drag coefficient more complex. The following section deals with the impact of all the influential parameters on the drag force coefficient in a unified manner. To minimize the effects of the experimental setup and the scale effect, only Thephanatos [31] (the best available) experimental data were implemented in this part.

The relationship between the drag coefficient and biofouling parameters was investigated by using the function fitting method with a minimization of the mean square error by the mean of a simplex algorithm. In order to reduce the complexity of the process, at this stage, one could decrease the number of parameters by assuming the effect of the aggregation (multi-layer effect) as a constant coefficient in the equation. The coefficient was calculated according to the information given by Thephanatos [31] and summarized in Figure 10. Despite all of these elaborations, the C_{Ds} of hard biofouling based on the best-fitted function can be estimated as:

$$C_{Ds} = M\left[1.3 - 0.76 \times e^{-14.5\left(\frac{k}{D}\right)} \times e^{-0.23(SC)}\right] \quad (2)$$

where k/D is the surface roughness ratio, SC is the surface coverage percentage (in %), and M is a constant. With multi-layers of biofouling, M is equal to 1.4 and for a single layer of biofouling, M is 1.0 [69].

In order to validate the proposed multi-parameters equation, all the gathered data have been applied and statistic parameters were calculated to compare the predicted C_{Ds} against the measured data. According to the statistical parameters, the calculated results are considered to be in agreement with the measured data (Figure 11). Figure 11 depicts all the statistical parameters in a Taylor diagram which is a mathematical diagram designed to graphically indicate whether the model of a system is realistic or not [70]. It is evident from the diagram that Equation (2) leads to the correlation coefficient of about 0.75, the root-mean-square error (RMS) error of about 0.15 and the standard deviation of 0.2, i.e., the model has a relatively reasonable correlation and low RMS error. However, the model results (point marked "A") have a slightly higher standard deviation rather than the "experimental data".

In order to visualize residual plots according to the multiple parameter model, Figure 12 is considered. It should be noted that the residual values were calculated only using Theophanatos [31] measured data; therefore, a lower number of measured data are available to calculate the residual value. Similar to the single parameter model (Figure 7), Figure 12a illustrates a one-mode histogram for the error with a symmetric bell-shaped around zero (the standard deviation of the residual values is about 0.06). It could be assumed to be normally distributed. The residuals of the fitted function (see the red dashed line in Figure 12b) has rather a constant trend which suggests that the error variance does not change by increasing the drag coefficient. One may conclude that the assumption of multiple parameters is likely to be a better approach to predict the drag force coefficient.

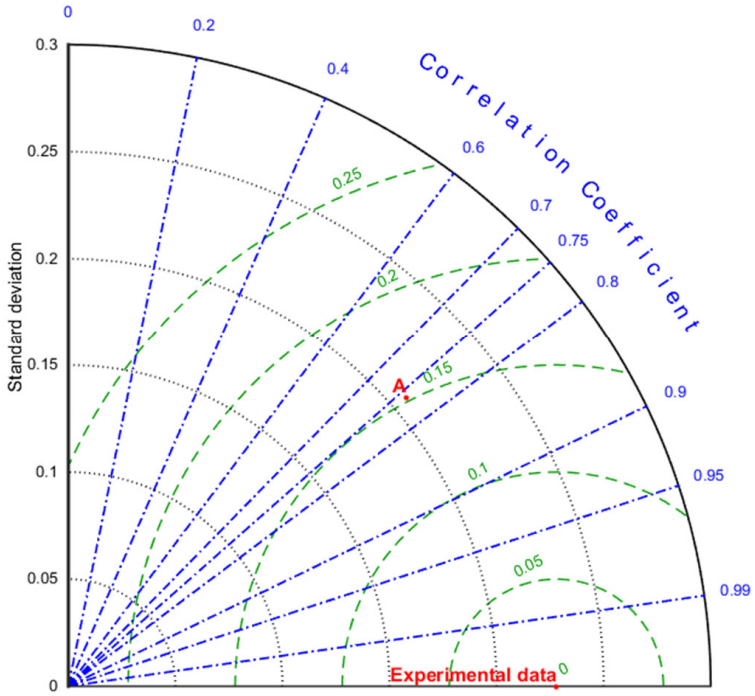

Figure 11. Statistical comparison of (Dashed blue: coorelation, Dashed black: standard deviation, Dashed green: RMS error) the current model estimates the C_D (the point "A") with observations of previous researchers (the point "Experimental data").

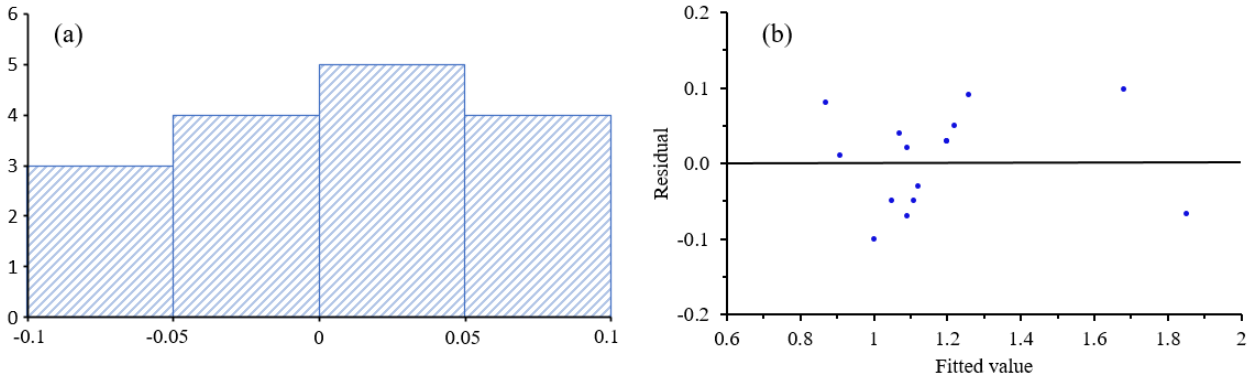

Figure 12. Residual plots of the multiple parameter model (**a**) residual histogram plot, (**b**) normal residual of the fitted curve (calculated value subtracted by measured value).

4. Conclusions and Remarks

4.1. Discussion

Despite the complexities, the new approach gives a better understanding of the effect of three parameters (percentage of coverage, multi-layer coverage and relative roughness) on the drag force coefficient in steady flow for hard fouling. Moreover, by using the proposed approach, an analytical model that respects the asymptotic behaviour and the physical meaning is proposed.

Considering these concerns, the multiple parameter equation was proposed as an adequate method for estimating the drag coefficient for circular members covered with biofouling and to assess the global error inherent to experimental tests, biological uncertainty, lack of definition of the roughness (no information of areal density of peaks) and in a lower proportion, to the numerical fitting. Taylor diagram has been shown to give a good overview of the good fitting of the experimental data by the model. The error of

modelling was also given in this paper; it is fundamental when propagating uncertainties in structural reliability assessment [22,71]. Additionally, for providing a more accurate model, it was shown that more tests for $k/D < 2.10^{-3}$ are needed. It corresponds to specific species (barnacles) or to an early stage development of others (mussels).

It must be pointed out that although the comparison of the estimated values with the experimental data verified the presented relationship for the existing gathered data published in the literature, the random nature of the phenomena and lack of measured data necessitates more investigations in this regard. First, it was shown that the uncertainty of the drag coefficient in the relationship falls below 5% if the roughness is fully defined (especially shape and areal distribution) [62]. Second, with more experiments, relationships should be provided as a function of the shape (species) and not only roughness.

4.2. Conclusions

In this paper, an intense review of the biofouling effect on hydrodynamic forces has been performed. The main concentration was on the drag force of fixed members under the steady/oscillating currents.

In general, this study tries to highlight the fact that hydrodynamic forces on cylindrical members could be significantly modified by introducing all of the pertinent marine fouling physical parameters. Most of the previous researchers calculated the drag coefficient of colonized cylinders, only based on the surface roughness ratio, particularly in the post-critical Re region. However, as proved in this paper, the dependency of biofouling only on the single parameter 'surface roughness' is subjected to a major debate. Therefore, although most models are relying only on the relative surface roughness, the C_{Ds} should be defined as a function of several parameters. It is also shown that the drag force coefficient depends upon surface coverage percentage, relative surface roughness, biofouling species, and the aggregation pattern.

In the second part of the paper, a new approach, relying on gathered data, is proposed to calculate the drag force coefficient based on surface roughness, surface coverage ratio, aggregation type as well as biofouling species. The method is straightforward, easy to understand, and well documented in the paper. However, the uncertainties of this approach are shown to be significant especially when the number of measured data is not sufficient enough. It means that the presented equation needs to be approved against the new measured data, however, this paper is much more emphasizing the methodology rather than the equation itself. It was shown that the error varies linearly with drag coefficients leading to a coefficient of variation of around 10%.

For an operational implementation in engineering, it should be noted that recent papers show that the uncertainty on the biofouling itself is significant and affect the reliability assessment [72]. That is particularly the case when assessing roughness [71] from on-site inspections [73–75]. In the future, similar studies can be performed by considering the inertia coefficient of the Morison equation.

Author Contributions: Conceptualization, F.S. and A.B.; methodology, F.S. and A.B.; software, A.B.; validation, F.S. and H.A.; formal analysis, A.B.; writing—original draft preparation, A.B.; writing—review and editing, F.S.; project administration, F.S.; funding acquisition, F.S. All authors have read and agreed to the published version of the manuscript.

Funding: Authors are grateful to Christian Berhault (senior Consultant), for their help in LEHERO-MG and ABIOP projects. This work was carried out within the project LEHERO-MG (Load Effect of HEterogeneous ROughness of Marine Growth) granted by WEAMEC, West Atlantic Marine Energy Community with the support of Région Pays de la Loire and in partnership with Naval Energies (Françoise Dubois).

Institutional Review Board Statement: Not applicable.

Informed Consent Statement: Not applicable.

Data Availability Statement: Not applicable.

Acknowledgments: This research was conducted in the framework of the West Atlantic Marine Energy Center–WEAMEC (LEHERO-MG project) and is supported by the French Region Pays de la Loire, Nantes Université, École Centrale de Nantes as well as CAPACITÉS SA. We thank also the APIOP+ project.

Conflicts of Interest: The authors declare no conflict of interest.

References

1. Zdravkovich, M.M. *Flow around Circular Cylinders*; Oxford Science Publications: New York, NY, USA, 2002.
2. Boukinda, M.L.; Schoefs, F.; Quiniou-Ramus, V.; Birades, M. Marine growth colonization process in guinea gulf: Data analysis. *J. Offshore Mech. Arct. Eng.* **2007**, *129*, 97–106. [CrossRef]
3. Ameryoun, H.; Schoefs, F. Probabilistic Modeling of Roughness Effects Caused by Bio-Colonization on Hydrodynamic Coefficients: A Sensitivity Study for Jacket-Platforms in the Gulf of Guinea. In *Offshore Technology*; ASME: New York, NY, USA, 2013; Volume 1, p. V001T01A057. [CrossRef]
4. Ameryoun, H. Probabilistic Modeling of Wave Actions on Jacket Type Offshore Wind Turbines in Presence of Marine Growth. Ph.D. Thesis, Université de Nantes Faculté des Sciences et des Techniques, Nantes, France, 2015.
5. Jusoh, I.; Wolfram, J. Effects of marine growth and hydrodynamic loading on offshore structures. *J. Mek.* **1996**, *1*, 77–96.
6. *API-RP-2A WSD*; Recommended Practice for Planning, Designing and Constructing Fixed Offshore Platforms-Working Stress Design. American Petroleum Institute: Washington, DC, USA, 2010.
7. Hiscock, K.; Tyler-Walters, H.; Jones, H. High Level Environmental Screening Study for Offshore Wind Farm Developments–Marine Habitats and Species Project. In *Report from the Marine Biological Association to the Department of Trade and Industry New & Renewable Energy Programme*; Report No. W/35/00632/00/00; Marine Biological Association: Plymouth, UK, 2002.
8. Shi, W.; Park, H.-C.; Baek, J.-H.; Kim, C.-W.; Kim, Y.-C.; Shin, H.-K. Study on the marine growth effect on the dynamic response of offshore wind turbines. *Int. J. Precis. Eng. Manuf.* **2012**, *13*, 1167–1176. [CrossRef]
9. Kerckhof, F.; Norro, A.; Jacques, T.; Degraer, S. Early colonisation of a concrete offshore windmill foundation by marine biofouling on the Thornton Bank (southern North Sea). In *Offshore Wind Farms in the Belgian Part of the North Sea: State of the Art after Two Years of Environmental Monitoring*; Degraer, S., Brabant, R., Eds.; Royal Belgian Institute for Natural Sciences, Management Unit of the North Sea Mathematical Models, Martien Ecosystem Management Unit: Brussels, Belgium, 2009; pp. 39–51.
10. Kerckhof, F.; Rumes, B.; Norro, A.; Jacques, T.G.; Degraer, S. Seasonal variation and vertical zonation of the marine biofouling on a concrete offshore windmill foundation on the Thornton Bank (southern North Sea). In *Offshore Wind Farms in the Belgian Part of the North Sea: Early Environmental Impact Assessment and Spatio-Temporal Variability*; Degraer, S., Brabant, R., Rumes, B., Eds.; Royal Belgian Institute for Natural Sciences, Management Unit of the North Sea Mathematical Models, Martien Ecosystem Management Unit: Brussels, Belgium, 2010; pp. 53–68.
11. Justesen, P. Hydrodynamic Forces on Large Cylinders in Oscillatory Flow. *J. Waterw. Port. Coast. Ocean Eng.* **1989**, *115*, 497–514. [CrossRef]
12. Kasahara, Y.; Koterayama, W.; Shimazaki, K. Wave Forces Acting on Rough Circular Cylinders at High Reynolds Numbers. In Proceedings of the Offshore Technology Conference Houston: Offshore Technology Conference, Houston, TX, USA, 6–9 May 2013; p. 12. [CrossRef]
13. Rodenbusch, G.; Källström, C. Forces On A Large Cylinder In Random Two-Dimensional Flows. In Proceedings of the Offshore Technology Conference Houston: Offshore Technology Conference, Houston, TX, USA, 5–8 May 1986; pp. 71–80. [CrossRef]
14. Sarpkaya, T. In-Line and Transverse Forces, on Cylinders in OsciIlatory Flow at High Reynolds Numbers. In Proceedings of the Offshore Technology Conference, Dallas, TX, USA, 3–6 May 1976; pp. 95–109.
15. Sarpkaya, T. *In-Line and Transverse Forces on Smooth and Sand-Roughened Cylinders in Oscillatory Flow at High Reynolds Numbers*; Technical Report; Naval Postgraduate School: Monterey, CA, USA, 1976.
16. Sarpkaya, T. *Vortex Shedding and Resistance in Harmonic Flow about Smooth and Rough Circular Cylinders at High Reynolds Numbers*; Technical Report; Naval Postgraduate School: Monterey, CA, USA, 1976.
17. Sarpkaya, T. On the Effect of Roughness on Cylinders. *J. Offshore Mech. Arct. Eng.* **1990**, *112*, 334. [CrossRef]
18. Theophanatos, A.; Wolfram, J. Hydrodynamic Loading on Macro-Roughened Cylinders of Various Aspect Ratios. *J. Offshore Mech. Arct. Eng.* **1989**, *111*, 214–222. [CrossRef]
19. Troesch, A.W.; Kim, S.K. Hydrodynamic forces acting on cylinders oscillating at small amplitudes. *J. Fluids Struct.* **1991**, *5*, 113–126. [CrossRef]
20. Schoefs, F.; Boukinda, M.L. Sensitivity Approach for Modelling Stochastic Field of Keulegan Carpenter and Reynolds Number Through a Matrix Response Surface. *J. Offshore Mech. Arct. Eng. JOMAE* **2004**, *132*, 1–7. [CrossRef]
21. Schoefs, F.; Ameryoun, H. Probabilistic Modeling of the Bio-Colonization Effects on Hydrodynamic Forces with Several Combinations of Sea-State Condition: A Study on Jacket-Platforms in the Gulf of Guinea. In *Offshore Technology*; ASME: Nantes, France, 2013; Volume 1, p. V001T01A056. [CrossRef]
22. Ameryoun, H.; Schoefs, F.; Barillé, L.; Thomas, Y. Stochastic modeling of forces on jacket-type offshore structures colonized by marine growth. *J. Mar. Sci. Eng.* **2019**, *7*, 158. [CrossRef]

23. Skaugset, K.; Baarholm, R. Effect of marine growth on an elastically mounted circular cylinder. In Proceedings of the ASME 2008 27th International Conference on Offshore Mechanics and Arctic Engineering, Estoril, Portugal, 15–20 June 2008; American Society of Mechanical Engineers: New York, NY, USA, 2008; pp. 855–861.
24. Baarholm, R.; Skaugset, K. Modelling and characterization of artificial marine growth. In Proceedings of the ASME 2008 27th International Conference on Offshore Mechanics and Arctic Engineering, Estoril, Portugal, 15–20 June 2008; pp. 863–870.
25. Nedrebø, E.L. Experimental Investigation of Marine Fouling on Piles in Currents. Master's Thesis, The Norwegian University of Science and Technology, Trondheim, Norway, 2014.
26. Resvanis, T.L.; Rao, Z.; Vandiver, J.K. Effects of strake coverage and marine growth on flexible cylinder VIV. In Proceedings of the ASME 2014 33rd International Conference on Ocean, Offshore and Arctic Engineering, New York, NY, USA, 30 June 2014; American Society of Mechanical Engineers: New York, NY, USA, 2014; p. V002T08A077.
27. Gaurier, B.; Germain, G.; Facq, J.V.; Baudet, L.; Birades, M.; Schoefs, F. Marine Growth Effects On The Hydrodynamical Behaviour Of Circular Structures. In Proceedings of the 14 emes Journées de l'Hydrodynamique, DGA Techniques Hydrodynamiques, Val du Reuil, France, 18–20 November 2014; p. 12.
28. Zeinoddini, M.; Bakhtiari, A.; Ehteshami, M.; Seif, M.S. Towards an understanding of the marine fouling effects on VIV of circular cylinders: Response of cylinders with regular pyramidal roughness. *Appl. Ocean Res.* **2016**, *59*, 378–394. [CrossRef]
29. Buresti, G. The effect of surface roughness on the flow regime around circular cylinders. *J. Wind Eng. Ind. Aerodyn.* **1981**, *8*, 105–114. [CrossRef]
30. Theophanatos, A. Marine Growth and Hydrodynamic Loading of Offshore Structures. Ph.D. Thesis, University of Strathclyde, Glasgow, UK, February 1988.
31. Zeinoddini, M.; Bakhtiari, A.; Schoefs, F.; Zandi, A.P. Towards an understanding of marine fouling effects on the vortex-induced vibrations of circular cylinders: Partial coverage issue. *Biofouling* **2017**, *33*, 268–280. [CrossRef] [PubMed]
32. Dürr, S.; Thomason, J. *Biofouling*; John Wiley and Sons: New York, NY, USA, 2009.
33. Wolfram, J.; Theophanatos, A. The Effects of Marine Fouling on the Fluid Loading of Cylinders: Some Experimental Results. In Proceedings of the Offshore Technology Conference, Houston, TX, USA, 6–9 May 1985. Paper Number: OTC-4954-MS.
34. Yan, T.; Yan, W.; Dong, Y.; Wang, H.; Yan, Y.; Liang, G. Marine fouling of offshore installations in the northern Beibu Gulf of China. *Int. Biodeterior. Biodegrad.* **2006**, *58*, 99–105. [CrossRef]
35. Kiu, K.Y.; Stappenbelt, B.; Thiagarajan, K.P. Effects of uniform surface roughness on vortex-induced vibration of towed vertical cylinders. *J. Sound Vib.* **2011**, *330*, 4753–4763. [CrossRef]
36. Mallick, M.; Kumar, A.; Murmu, A. Flow Modeling in Various Cylindrical Surfaces. *Aquat. Procedia* **2015**, *4*, 834–840. [CrossRef]
37. Achenbach, E.; Heinecke, E. On vortex shedding from smooth and rough cylinders in the range of Reynolds numbers 6×10^3 to 5×10^6. *J. Fluid Mech.* **1981**, *109*, 239–251. [CrossRef]
38. Bearman, P.W.; Harvey, J.K. Control of circular cylinder flow by the use of dimples. *AIAA J.* **1993**, *31*, 1753–1756. [CrossRef]
39. Fuss, F.K. The effect of surface skewness on the super/post-critical coefficient of drag of roughened cylinders. *Procedia Eng.* **2011**, *13*, 284–289. [CrossRef]
40. Islam, T.; Hassan, S.R. Experimental and numerical investigation of flow over a cylinder at Reynolds number 10^5. *J. Mod. Sci. Technol.* **2013**, *1*, 52–60.
41. Butt, U.; Egbers, C. Aerodynamic characteristics of flow over circular cylinders with patterned surface. *J. Mater. Mech. Manuf.* **2013**, *1*, 121. [CrossRef]
42. Molin, B. *Hydrodynamique Des Structures Offshore*; Editions Technip: Paris, France, 2002.
43. Goff, J.E. A review of recent research into aerodynamics of sport projectiles. *Sports Eng.* **2013**, *16*, 137–154. [CrossRef]
44. Nath, J.H. Heavily roughened horizontal cylinders in waves. In Proceedings of the Conference on Behaviour of Offshore Structures; Oregon State University: Corvallis, OR, USA, 1982; Volume 1, pp. 387–407.
45. Ribeiro, J.D. Effects of surface roughness on the two-dimensional flow past circular cylinders I: Mean forces and pressures. *J. Wind Eng. Ind. Aerodyn.* **1991**, *37*, 299–309. [CrossRef]
46. Basu, R.I. Aerodynamic forces on structures of circular cross-section. Part 1. Model-scale data obtained under two-dimensional conditions in low-turbulence streams. *J. Wind Eng. Ind. Aerodyn.* **1985**, *21*, 273–294. [CrossRef]
47. Achenbach, E. Influence of surface roughness on the cross-flow around a circular cylinder. *J. Fluid Mech.* **1971**, *46*, 321–335. [CrossRef]
48. Achenbach, E. The effect of surface roughness on the heat transfer from a circular cylinder to the cross flow of air. *Int. J. Heat Mass Transf.* **1977**, *20*, 359–369. [CrossRef]
49. Güven, O.; Farell, C.; Patel, V.C. Surface-roughness effects on the mean flow past circular cylinders. *J. Fluid Mech.* **1980**, *98*, 673–701. [CrossRef]
50. Nakamura, Y.; Tomonari, Y. The effects of surface roughness on the flow past circular cylinders at high Reynolds numbers. *J. Fluid Mech.* **1982**, *123*, 363–378. [CrossRef]
51. Rooney, D.M.; Peltzer, R.D. The effects of roughness and shear on vortex shedding cell lengths behind a circular cylinder. *ASME Trans.* **1982**, *104*, 72–80. [CrossRef]
52. Jubran, B.A.; Hamdan, M.N.; Al Bedoor, B.O. Roughness and turbulence intensity effects on the induced flow oscillation of a single cylinder. *Appl. Sci. Res.* **1992**, *49*, 101–115. [CrossRef]

53. Ribeiro, J.D. Effects of surface roughness on the two-dimensional flow past circular cylinders II: Fluctuating forces and pressures. *J. Wind Eng. Ind. Aerodyn.* **1991**, *37*, 311–326. [CrossRef]
54. Cheung, J.C.K.; Melbourne, W.H. Effects of surface roughness on a circular cylinder in supercritical turbulent flow. In Proceedings of the Twelfth Australian Fluid Mechanics Conference, Sydney, Australia, 4–8 December 1995.
55. Uematsu, Y.; Yamada, M. Effects of aspect ratio and surface roughness on the time-averaged aerodynamic forces on cantilevered circular cylinders at high Reynolds numbers. *J. Wind Eng. Ind. Aerodyn.* **1995**, *54*, 301–312. [CrossRef]
56. Wolfram, J.; Naghipour, M. On the estimation of Morison force coefficients and their predictive accuracy for very rough circular cylinders. *Appl. Ocean Res.* **1999**, *21*, 311–328. [CrossRef]
57. Gao, Y.; Fu, S.; Wang, J.; Song, L.; Chen, Y. Experimental study of the effects of surface roughness on the vortex-induced vibration response of a flexible cylinder. *Ocean Eng.* **2015**, *103*, 40–54. [CrossRef]
58. Zhou, B.; Wang, X.; Gho, W.M.; Tan, S.K. Force and flow characteristics of a circular cylinder with uniform surface roughness at subcritical Reynolds numbers. *Appl. Ocean Res.* **2015**, *49*, 20–26. [CrossRef]
59. Marty, A.; Schoefs, F.; Damblans, G.; Facq, J.-V.; Gaurier, B.; Germain, G. Experimental comparative study of two kinds of hard marine growth effects on the hydrodynamical behaviour of a cylinder submitted to wave and current solicitations. *Ocean Eng.* 2022; *in press*.
60. Marty, A.; Berhault, C.; Damblans, G.; Facq, J.-V.; Gaurier, B.; Germain, G.; Soulard, T.; Schoefs, F. Experimental study of marine growth effect on the hydrod-ynamical behaviour of a submarine cable. *Appl. Ocean Res.* **2021**, *114*, 102810. [CrossRef]
61. Marty, A.; Schoefs, F.; Soulard, T.; Berhaul, C.; Facq, J.-V.; Gaurier, B.; Germain, G. Effect of roughness of mussels on cylinder forces from a realistic shape modelling. *J. Mar. Sci. Eng. Sect. Ocean Eng.* **2021**, *9*, 558. [CrossRef]
62. Batham, J.P. Pressure distributions on circular cylinders at critical Reynolds numbers. *J. Fluid Mech.* **1973**, *57*, 209–228. [CrossRef]
63. Schoefs, F. Sensitivity approach for modeling the environmental loading of marine structures through a matrix response surface. *Reliab. Eng. Syst. Saf.* **2008**, *93*, 1004–1017. [CrossRef]
64. Vedaprakash, L.; Dineshram, R.; Ratnam, K.; Lakshmi, K.; Jayaraj, K.; Babu, S.M.; Venkatesan, R.; Shanmugama, A. Experimental studies on the effect of different metallic substrates on marine biofouling. *Colloids Surf. B Biointerfaces* **2013**, *106*, 1–10. [CrossRef]
65. Wolfram, J.; Jusoh, I.; Sell, D. Uncertainty in the estimation of fluid loading due to the effects of marine growth. In Proceedings of the 12th International Conference on Offshore Mechanics & Arctic Engineering, OMAE, Glasgow, UK, 20–24 June 1993.
66. Morkovin, M.V. On Roughness—induced transition: Facts, Views, and speculations. In *Instability and Transition*; Springer: New York, NY, USA, 1990; pp. 281–295.
67. DNV. *Recommended Practice DNV-RP-C205. Environmental Conditions and Environmental Loads*; Det Norske Veritas: Hovik, Norway, 2017.
68. Schoefs, F.; Boukinda, M.; Guillo, C.; Rouhan, A. Fatigue of jacket platforms: Effect of marine growth loading. In Proceedings of the 24th International Conference on Offshore Mechanics and Arctic Engineering, Halkidiki, Greece, 12–16 June 2005.
69. Bakhtiari, A.; Schoefs, F.; Ameryoun, H. A unified approach for estimating of the drag coefficient in offshore structures in presence of bio-colonization. In Proceedings of the 37th International Conference on Ocean, Offshore & Arctic Engineering, Madrid, Spain, 17–22 June 2018.
70. Taylor, K.E. Summarizing multiple aspects of model performance in a single diagram. *J. Geophys. Res. Atmos.* **2001**, *106*, 7183–7192. [CrossRef]
71. Schoefs, F.; O'Byrne, M.; Pakrashi, V.; Gosh, B.; Oumouni, M.; Soulard, T.; Reynaud, M. Fractal Dimension as an Effective Feature for Characterizing Hard Marine Growth Roughness from Underwater Image Processing in Controlled and Uncontrolled Image Environments. *J. Mar. Sci. Eng.* **2021**, *9*, 1344. [CrossRef]
72. Schoefs, F.; Tran, B. Reliability updating of offshore structures subjected to marine growth. *Energies* **2022**, *15*, 414. [CrossRef]
73. O'Byrne, M.; Schoefs, F.; Pakrashi, V.; Ghosh, B. An underwater lighting and turbidity image repository for analysing the performance of image based non-destructive techniques. *Struct. Infrastruct. Eng.* **2018**, *14*, 104–123. [CrossRef]
74. O'Byrne, M.; Pakrashi, V.; Schoefs, F.; Ghosh, B. Semantic Segmentation of Underwater Imagery Using Deep Networks. *J. Mar. Sci. Eng.* **2018**, *6*, 93. [CrossRef]
75. O'Byrne, M.; Pakrashi, V.; Schoefs, F.; Ghosh, B. Applications of Virtual Data in Subsea Inspections. *J. Mar. Sci. Eng.* **2020**, *8*, 328. [CrossRef]